Photoinduced oxidative degradation of unsaturated $M_3(dppm)_3CO^{2+}$ clusters (M = Pd, Pt) by chlorocarbons and chloride ion

Pierre D. Harvey, Réjean Provencher, Jonathan Gagnon, Tianle Zhang, Daniel Fortin, Karine Hierso, Marc Drouin, and Steve M. Socol

Abstract: Both $M_3(dppm)_3CO^{2+}$ clusters (M = Pd, Pt) photoreact with chlorocarbons (Cl—R; R = CCl_3, $CHCl_2$, CH_2Cl, C_6H_5, $C_{10}H_{15}$ (adamantyl)) and chloride ion (slowly) to produce the oxidized mononuclear species $M(dppm)Cl_2$ as a sole isolated M-coordinated inorganic product. Such reactions do not proceed in the dark, except for R = $CH_2C_6H_5$. Among the organic products, the coupling compound R–R (R = C_6H_5) is observed along with many phosphine compounds such as $P(C_6H_5)_3$. In an attempt to elucidate the photoinduced mechanism at the early stage of the phototransformations, the following have been investigated : the ground state binding constants (K_{11} for M = Pd in methanol), the photochemical quantum yields of cluster disappearance (Φ_{dis} for M = Pd) as a function of substrates, substrate concentrations, excitation wavelengths, solvents (ethanol vs toluene), and presence of CO, and the emission lifetimes (τ_e for M = Pt) at 77 K as a function of substrate concentrations (CH_2Cl_2 and $CHCl_3$) in ethanol and toluene. Some of the experimental conclusions have also been corroborated theoretically using density functional theory. Geometry optimization calculations have been performed for the model compounds $Pd_3(PH_3)_6CO^{2+}\cdots Cl^-$, $Pd_3(PH_3)_6{}^{2+}$, $Pd_3(PH_3)_6CO^{2+}\cdots Cl^0$, $Pd_3(PH_3)_6CO^{2+}\cdots Cl\text{-}CH_3$, and $Pd_3(PH_3)_6CO^{3+}$ in their ground states.

Key words: atom abstraction, photochemistry, C-Cl bond, clusters, host-guest.

Résumé : Les agrégats $M_3(dppm)_3CO^{2+}$ (M = Pd, Pt) photoréagissent tous les deux avec les chlorocarbones (Cl-R; CCl_3, $CHCl_2$, CH_2Cl, C_6H_5, $C_{10}H_{16}$ (adamantyle)) et avec l'ion chlorure (lentement) pour conduire à des espèces mononucléaires oxydées $M(dppm)Cl_2$ qui correspondent au seul produit inorganique M-coordiné à être isolé. Ces réactions ne se produisent pas à la noirceur, excepté pour le composé R = $CH_2C_6H_5$. Parmi les composés organiques, on observe le composé de couplage R–R (R = C_6H_5) ainsi que plusieurs phosphines telle que la $P(C_6H_5)_3$. Dans le but d'élucider le mécanisme photoinduit dans l'étape initiale des phototransformations, on a examiné les caractéristiques suivantes : les constantes d'association dans l'état fondamental (K_{11}, pour M = Pd dans le méthanol), les rendements quantiques photochimiques pour la disparition des agrégats (Φ_{dis} pour M = Pd) en fonction des substrats, des concentrations de substrat, des longueurs d'onde d'excitation, des solvants (éthanol vs. toluène) et de la présence de CO et les durées de vie d'émissions (τ_e pour M = Pt), à 77 K, en fonction des concentrations de substrat (CH_2Cl_2 et $CHCl_3$) dans l'éthanol et le toluène. Un certain nombre de conclusions expérimentales ont aussi été corroborées d'une façon théorique en faisant appel à la théorie de la densité fonctionnelle. On a effectué des calculs d'optimisation de géométrie pour les composés modèles $Pd_3(PH_3)_6CO^{2+}\cdots Cl^-$, $Pd_3(Ph_3)_6{}^{2+}$, $Pd_3(PH_3)_6CO^{2+}\cdots Cl^0$, $Pd_3(PH_3)_6CO^{2+}\cdots Cl\text{-}CH_3$ et $Pd_3(PH_3)_6CO^{3+}$ dans leurs états fondamentaux.

Mots clés : enlèvement d'atome, photochimie, liaison C—Cl; agrégats, hôte–invité.

[Traduit par la rédaction]

Introduction

The photoinduced oxidation of bi- and polynuclear organometallic complexes has been a topic of long term interest (1). The two possible mechanisms are the electron transfer from the excited complex to the substrate, and the atom transfer from the substrate to the excited complex (1). These key processes occur in the early stage of the transformations, and the elucidation of which mechanism is proceeding requires carefully designed experiments. In metal–metal bonded complexes, another pathway is possible, and involves photoinduced homolytic metal–metal bond scission in the excited states (1), generating radical species that exhibit redox and atom transfer properties that are different from those of the ground state metal–metal bonded species. Relevant to this study are recent photochemical and spectroscopic studies reported by our group (2, 3) and others (4, 5) on low-valent Pd–Pd bonded isocyanide complexes, and which have demonstrated the rich photochemistry that these species offer and the diversity of primary photoinduced processes that have been observed. More recently, our group has been interested in the photoactivation of small molecules, notably $O_2(g)$ by the low-valent $Pd_3(dppm)_3CO^{2+}$ cluster (dppm = $((C_6H_5)_2P)_2CH_2$) (6).

Received February 6, 1996.

This paper is dedicated to Professor Howard C. Clark in recognition of his contributions to Canadian chemistry.

P.D. Harvey,[1] R. Provencher, J. Gagnon, T. Zhang, D. Fortin, K. Hierso, M. Drouin,[2] and S.M. Socol. Département de chimie, Université de Sherbrooke, Sherbrooke, QC J1K 2R1, Canada.

[1] Author to whom correspondence may be addressed. Telephone: (819) 821-7092. Fax: (819) 821-8017. E-mail: pharvey@structure.chimie.usherb.ca

[2] Laboratoire de chimie structurale.

[3] Present address: Southern Utah University, Department of Physical Sciences, Cedar City, UT 84720, U.S.A.

Can. J. Chem. **74**: 2268–2278 (1996). Printed in Canada / Imprimé au Canada

The observed product was the $Pd_3(dppm)_3(O_2)_2^{2+}$ species, which was formed with a quantum yield efficiency of about 3% (at λ_{exc} ~500 nm). This work extends the photochemistry of the $M_3(dppm)_3CO^{2+}$ clusters (M = Pd, Pt) towards the activation of chlorocarbon molecules, and provides a series of experiments that help elucidate the possible mechanisms responsible for the phototransformations *at the early stage* of the photoinduced processes. Density functional theory is also used in order to corroborate some of the experimental findings by the means of geometry optimization computations of some proposed intermediate species. This work will provide experimental evidence for a double- pathway mechanism, one involving a photoinduced Cl atom abstraction followed by a degradation of the cluster, and another involving a fragmentation followed by subsequent reaction with the chlorocarbon molecules.

Experimental

Materials

$[Pd_3(dppm)_3CO](Y = CF_3CO_2,PF_6)_2$ (7) and $[Pt_3(dppm)_3CO](PF_6)_2$ (8) were prepared according to literature procedures. Methanol (BDH), dichloromethane (BDH), chloroform (BDH), carbon tetrachloride (Anachemia), sodium chloride (Fisher), benzyl chloride (Aldrich Chem. Co.), chlorobenzene (BDH), and 1-chloroadamantane (1-Cl-ada; Aldrich Chem. Co.) were purchased at the highest purity grade possible (eg., spectrograde) and were used as received. Ethanol (Les alcools de commerces, 95%) and toluene (BDH) were dried over Na(s) and distilled by fractionation. The formation of a glass at 77 K, with no sign of cracking, was used as the test of solvent dryness.

The complex $[Pd_3(dppm)_3(CO)(N_2C_6H_4NEt_2)](CF_3CO_2)_2(BF_4)$ was prepared via a direct reaction between $[Pd_3(dppm)_3CO](CF_3CO_2)_2$ and the diazonium salt $[\mathit{para}\text{-}N_2C_6H_4NEt_2](BF_4)$ (Aldrich Chem. Co) in methanol in a 1:1 stoichiometric ratio for 2–3 h. The complex has been characterized by IR ($\nu(\mathrm{N{\equiv}\overset{+}{N}})$ = 2162 cm^{-1}, $\nu(CO)$ = 1830 cm^{-1} (solid state)); ^1H NMR ($\delta(CH^aH^bP_2)$: 4.75 and 4.98 ppm (AB quartet; $^2J(H^aH^b)$ = 15 Hz in $(CD_3)_2CO$)), and UV visible spectroscopy (λ_{max} = 464 (br), 380, and 308 nm). The complex $[Pd_3(dppm)_3(CO)(Cl)]BF_4{\cdot}2CH_2Cl_2$ was prepared from daylight irradiation of $[Pd_3(dppm)_3(CO)N_2C_6H_4NEt_2](CF_3CO_2)_2(BF_4)$ in neat CH_2Cl_2. This reaction does not proceed in the dark. The product was characterized by X-ray crystallography using single crystals formed during the photoreaction as CH_2Cl_2 solvate. Its report is appropriate at this time for the purpose of this work (supplementary material, see footnote 4). The full characterization and investigation of the diazonium adducts will be reported in due course.

Instrumentation

The emission spectra were measured on a PTI LS 100 spectroflurometer. The emission lifetimes (τ_e) were measured on the same instrument fitted with a tungsten EG & G model FX-280 microsecond flash-lamp source (~1 μs fwhm) and a phosphorimeter component. To obtain data that are of sufficient quality for this work, multi-scanning and pulsing techniques were employed.

Photochemical studies

The photochemical reactions were performed with a home-made immersion cell using an Ace Hanovia Hg–Xe 200-W lamp. The photoreactions proceeded with broadband irradiation using a uranium sleeve glass filter (λ_{cutoff} ~340 nm). For the quantum yield measurements, ferrioxalate actionometry was employed (9–11). The actinometer excitation slits were set at 0.5 mm, and excitation was set at 488 nm for all samples and standards unless stated otherwise. The excitation wavelength was selected using a Aminco-Bomem monochromator, also equipped with a Hg–Xe 200-W lamp. The absorbance of the complex and standard solutions was adjusted to a value of ~0.4–0.5 at λ_{max} ~487 nm for M = Pd and at λ_{max} ~380 nm for M = Pt prior the measurements. Typical concentrations range from 1.5×10^{-5} to 2.0×10^{-5} M. The calibrations of the standard ferrioxalate actinometric solutions were performed carefully in the dark. The absorbance change at a given irradiation time was followed by UV–visible spectroscopy (Hewlett–Packard 8452A) at a value of λ_{max} that varied between 466 and 490 nm depending upon the nature of the solvent mixture. All measurements and calibration experiments were performed at least 3 times and before 10% photoconversion.

Binding Constant Measurements

The K_{11} measurements were performed by UV–visible spectroscopy (12) at room temperature, and were extracted by plotting the Benesi–Hildebrand graphs (~$1/\Delta A$ vs. 1/[substrate] with ΔA as the absorbance change upon the increase in substrate concentration). The ratio intercept/slope in this plot gives K_{11}. As a counter check, the K_{11} values were also evaluated using Scatchard and Scott plots ($-\Delta A$/[substrate] vs. $-\Delta A$, $K_{11} = -$slope (Scatchard); $-$[substrate]/ΔA vs. [substrate], K_{11} = slope/intercept (Scott)). The measured K_{11} values are all found to be the same within the experimental uncertainties, generally ±10% based upon the maximum and minimum values obtained, except for the Cl^- ion, which turned out to be irreproducible (see text below). Typically between 6 and 10 data points were acquired for each measurement, which was repeated three times. Details on the methodology employed can be found in ref. 13.

Computational details

The reported density functional calculations were all carried out utilizing the program called Amsterdam Density Functional that was developed by Baerends et al. (14, 15) and vectorized by Raveneck (16). The numerical integration procedure applied for the calculations was developed by te Velde and co-workers (17). The geometry optimization procedure was based on the method developed by Versluis and Ziegler (18). The electronic configurations of the molecular systems were described by an uncontracted double-ζ basis set (19) on palladium for 4*s*, 4*p*, and 5*s*, and triple-ζ for 5d. Double- ζ STO basis sets (20) were used for chloride (3*s*, 3*p*), phosphorus (3*s*, 3*p*), oxygen (2*s*, 2*p*), carbon (2*s*, 2*p*), and hydrogen (1*s*), augmented with a single 4*d* polarization function for Cl and P, a single 3*d* one for O, and C, and a 2*p* function for H. No polarization function was used for palladium. The $1s^2\ 2s^2\ 2p^6\ 3s^2\ 3d^{10}$ configuration on palladium, the $1s^2$ $2s^2$ configuration on chloride and on phosphorus, and the $1s^2$ configurations on oxygen, carbon, and nitrogen were treated by the frozen-core approximation (15). A set of auxiliary (21) *s*, *p*, *d*, *f*, and *g* STO functions, centered on all nuclei, was used in order to fit the molecular density and present Coulomb and exchange potentials accurately in each SCF cycle. Energy differences were calculated by including the local exchange-correlation potential by Vosko et al. (22). No nonlocal exchange and correlation corrections were made for the geometry optimizations.

Crystal structure of $[Pd_3(dppm)_3(\mu\text{-}CO)(\mu\text{-}Cl)](BF_4)\cdot CH_2Cl_2$

Intensity data were collected at 190 K on an Enraf–Nonius CAD-4 automatic diffractometer using graphite monochromated Mo$K\alpha$ radiation. The NRCCAD (23*a*) programs were used for centering, indexing, and data collection. The unit cell dimensions were obtained by least-squares fit of 24 centered reflections in the range of $30° \leq 2\theta \leq 36°$. During data collection, the intensities of two standard reflections were monitored every 60 min. No significant decay was observed. The structure was solved by the application of direct methods using the NRCVAX (23*b*) program and refined by least squares. The atomic scattering factors in stored NRCVAX are from Cromer and Waber (International tables for X-ray crystallography, Vol IV). Hydrogen atoms were geometrically placed at idealized position and not refined. At convergence the final discrepancy indices were $R = 0.063$, $wR = 0.066$, and $SC = 1.55$. The residual positive and negative electron densities in the final maps were 1.27 and -1.67 e/Å^3 and were located in the vicinity of the BF_4^- anion. The C=O bond distance was fixed at 1.15 Å in the refinement. The ORTEP (23*c*) diagram was generated from NRCVAX. The crystal has one solvent molecule (CH_2Cl_2). The BF_4^- molecule is disordered and was treated as a B atom surrounded by two interlocking ideal tetrahedra of F atoms (all U_{ij} restrained to be equal) with B---F distances restrained to 1.36 Å; a 63:37 occupancy ratio is observed. Only the higher occupancy site was retained. Restrain refinement was used on U_{ij} to be all equal for C1 to C6 atoms because of thermal motion leading to large U parameters.

Results and discussion

1. Photoreactions

The $M_3(dppm)_3CO^{2+}$ clusters undergo photooxidative degradation in the presence of chlorocarbons either as a neat solvent or in acetonitrile solutions, and also in the presence of Cl^- ions. These photoinduced chemical processes form the known corresponding $M(dppm)Cl_2$ complexes as sole isolated metal-coordinated inorganic products (for M = Pd, Pt) as identified from comparison of ^1H and ^{31}P NMR spectra with authentic samples (eq. [1]).

$$[1] \quad M_3(dppm)_3CO^{2+} \xrightarrow[h\nu]{\text{R-Cl or Cl}^-} M(dppm)Cl_2$$

The reactions do not proceed in the dark. To establish the mechanistic step of the $Pd_3(dppm)_3CO^{2+}$ photoconversion to $Pd(dppm)Cl_2$, the model system $Pd_3(dppm)_3(CO)(Y)^{3+}$ (Y = $N_2C_6H_4NEt_2$) (13) was investigated. This compound is prepared from the binding of $Pd_3(dppm)_3CO^{2+}$ with $[N_2C_6H_4NEt_2]^+$ (as the BF_4^- salt) (13). This complex is surprisingly unstable to light in the presence of CH_2Cl_2 to slowly form $[Pd_3(dppm)_3(CO)(Cl)]BF_4$ as identified by X-ray crystallography (as a CH_2Cl_2 solvate). This cationic cluster is essentially identical to that reported by Puddephatt and co-workers (24) and the bulk of the data have been deposited as supplementary material.[4] Only minor structural differences have been noticed such as the absence of disorder between the Cl^- ion and CO group, and minor changes in bond lengths and angles. Further light irradiation of the cluster also forms $Pd(dppm)Cl_2$. This later photoreaction is significantly slower. Based upon these observations, it is believed that this Cl^- adduct species may be one of the intermediate products prior to the formation of the final oxidized mononuclear $M(dppm)Cl_2$ complex.

By GC–MS, one of the organic products was identified as biphenyl for the chlorobenzene substrate. Possibly due to volatility problems, the expected ethylene and acetylene products for dichloromethane and chloroform were not observed under the same experimental conditions. The presence of biphenyl indicates the formation of the highly reactive radical phenyl group. Numerous other organics (for M = Pd) are also unselectively photoproduced, but their identity is not known at this time. This was not the purpose of this work. By GC–MS, the molecular weights of the fragments indicate that large organic molecules have been generated, along with various phosphine-containing compounds such as $P(C_6H_5)_3$. For the Cl^- substrates, the photolyses are very slow and only $Pd(dppm)Cl_2$ and dppm decomposition products are observed (as expected). There was no evidence of acetonitrile solvent participation in the products.

2. Thermodynamics

The emission spectra of the $M_3(dppm)_3CO^{2+}$ clusters reveal that the triplet energies (E_T) are determined from emission band maxima, located at 1.76 eV (14 200 cm^{-1}, M = Pd) and 1.91 eV (16 100 cm^{-1}, M = Pt) (25). From cyclic voltammetry, both clusters exhibit an irreversible electrochemical oxidation wave at +1.38 V and +1.05 V vs. SCE for the $Pd_3(dppm)_3CO^{2+}$ and $Pt_3(dppm)CO^{2+}$, respectively, both as PF_6^- salts, in degassed acetonitrile solutions containing 0.1 M tetrabutylammonium hexafluorophosphate. The coulometric experiments establish that the electrochemical process is a multielectron process, which places an upper limit for the one-electron oxidation of the clusters (i.e., $\leq$+1.38 V (M = Pd) and $\leq$+1.05 V (M = Pt) vs. SCE). The excited state driving forces in the lowest energy triplet excited state ($E^{*/+}$) would then be evaluated to be in the order of 0.38 V and 0.86 V vs. SCE for M = Pd and Pt, respectively. These values are not great enough to spontaneously reduce most simple chlorocarbons such as C_6H_5Cl ($E^{0/-} = -2.32$ V vs. NHE), CH_2Cl_2 ($E^{0/-} = -2.23$ V vs. NHE), $CHCl_3$ ($E^{0/-} = -1.67$ V vs. NHE), and CH_3Cl ($E^{0/-} = -2.23$ V vs. NHE) (26). In these cases, the photoinduced electron transfer mechanism from the $M_3(dppm)_3CO^{2+}$ cluster in their lowest energy $^3A_2$ states to the chlorocarbon molecules is clearly thermodynamically unfavorable. This is obviously also true for the cluster oxidation in the presence of the Cl^- anion. Con-

---

[4] Copies of material on deposit may be purchased from: The Depository of Unpublished Data, Document Delivery, CISTI, National Research Council Canada, Ottawa, Canada K1A 0S2. These data, with the exemption of anisotropic thermal parameters and torsion angles, have also been deposited with the Cambridge Crystallograhic Data Centre, and can be obtained on request from The Director, Cambridge Crystallograhic Data Centre, University Chemical Laboratory, 12 Union Road, Cambridge, CB2 1EZ, U.K.

Fig. 1. Typical UV–visible spectroscopic changes when additions of $CHCl_3$ are made to a solution of $Pd_3(dppm)_3CO^{2+}$ in methanol at 298 K ([cluster] ~1 × 10^{-5} M).

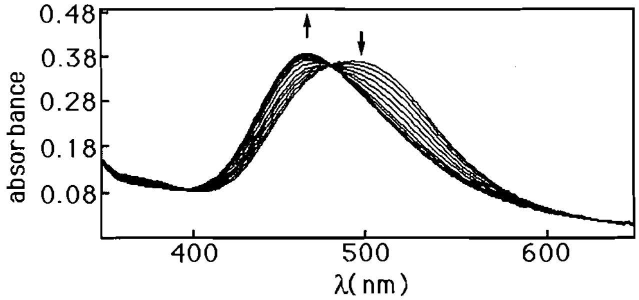

Scheme 1.

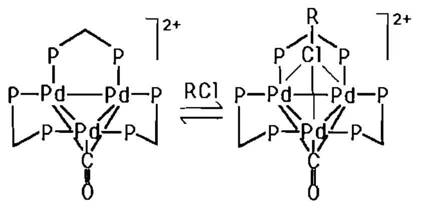

versely, substrates such as $C_6H_5CH_2Cl$ ($E^{o/-} = -1.0$ V vs. SCE (27)) and CCl_4 ($E^{0/-} = -0.78$ and -1.67 V) offer the possibility that such a photoinduced process occurs for $Pt_3(dppm)_3CO^{2+}$. For CCl_4, the presence of a fourth Cl atom renders the molecule an excellent electron scavenger. For $C_6H_5CH_2Cl$, scission of the reduced species generates the Cl^- ion and the benzyl radical ($C_6H_5{\cdot}CH_2$), which is stabilized by resonance. In these cases, electron transfer could also be considered.

3. Binding studies

From a thermodynamic standpoint, a photoinduced atom abstraction mechanism must be considered. In such a mechanism, the substrate R—Cl *must* physically approach the excited M_3^{2+} center. Recently published flash photolysis measurements indicate that the excited state lifetimes range from 25 (M = Pd) to a few hundred picoseconds (M = Pt) (25), which are not long enough to allow a diffusion of the $M_3(dppm)_3CO^{2+*}$ ($^3A_2$) species to the substrates. The photoprocess (atom abstraction) must be *unimolecular*, involving a ground state preassembling of the clusters and the substrates. Since the chromophoric unsaturated M_3^{2+} center is located at the bottom of a cavity formed by six dppm-phenyl groups, the substrate must act as a guest molecule in this pocket.

This section addresses the ground state host–guest behavior of the $M_3(dppm)_3CO^{2+}$–chlorocarbon systems. The cluster of choice is $Pd_3(dppm)_3CO^{2+}$ since its absorption spectrum exhibits a well-defined absorption band at around 480 nm, where isosbestic points can be clearly observed upon association with a substrate (13). Methanol was chosen as solvent since previous studies established that this solvent interacts the least with the cavity (13), and offers good solubility for the cluster and substrates.

Figure 1 shows UV–visible spectra changes upon addition of chloroform. Clear isosbestic points are evident at ~479 and ~398 nm, indicating a 1:1 stoichiometric ratio (Scheme 1).

Fig. 2. Typical Benesi–Hildebrand, Scatchard, and Scott plots associated with the addition of $CHCl_3$ to a solution of $Pd_3(dppm)_3CO^{2+}$ in methanol at 298 K.

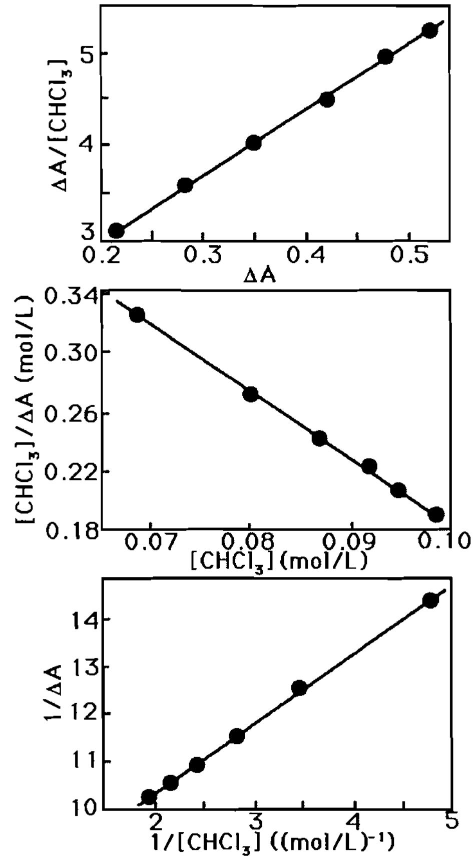

The K_{11} values extracted from the Benesi–Hildebrand plots (Fig. 2) are listed in Table 1. These constants have also been verified by also extracting them from the Scatchard and Scott plots (Fig. 2). Except for Cl^-, reversibility can be observed from the displacement of the substrate by adding a second substrate monitoring the progression by UV–visible spectroscopy (each substrate exhibits its own λ_{max}). In the Cl^- case, the binding constant is very large (>10 000 M^{-1}) and somewhat hard to obtain with precision. There is no obvious trend between the molecular dimension and K_{11} (Table 1). However, some rationalization can be made. Chloride is the smallest substrate of this series and is charged ($Cl^- \cdots Pd_3^{2+}$); it is the most efficient guest of the series. C_6H_5Cl compares structurally to toluene, which was investigated earlier ($K_{11} = 0.08 \pm 0.02$ M^{-1} (13)). The slight increase in K_{11} here ($K_{11} = 0.16 \pm 0.01$ M^{-1}) could be associated with some extra binding between the Cl atom and the Pd_3 center. Furthermore, adding extra Cl atoms on a given substrate should then slightly increase K_{11} if the substrate is not too sterically demanding. This is indeed observed for CH_2Cl_2 (0.25 ± 0.03 M^{-1}) and $CHCl_3$ (4.9 ± 0.5 M^{-1}). However, a slight decrease is observed for CCl_4 (3.4 ± 0.1 M^{-1}), which could be due to the slight increase in molecular dimensions.

Two unexpected results come from 1-Cl-ada (35 ± 5 M^{-1}) and $C_6H_5CH_2Cl$ (7.3±0.1 M^{-1}), which were used for their bulkiness (1-Cl-ada), and low bond dissociation energy and reduction potential ($C_6H_5CH_2Cl$), respectively. The increase

Table 1. Comparison of K_{11} values and substrate sizes.

Substrate	K_{11}/M^{-1}[a]	Dimensions[b]
Cl^-	[c]	van der Waals diam. = 3.6 Å, ionic diam. = 3.4 Å
CH_3Cl	Not measured	Average diameter ~4.7 Å
CH_2Cl_2	0.25 ± 0.03	Average diameter ~5.2 Å
$CHCl_3$	4.9 ± 0.5	Average diameter ~5.7 Å
CCl_4	3.4 ± 0.1	Average diameter ~6.1 Å
1-Cl-ada	35 ± 5	Average diameter ~6.5 Å
C_6H_5Cl[d]	0.16 ± 0.1	Assuming a rectangular shape ~8.7 × 3.6 × 6.9 Å
$C_6H_5CH_2Cl$	7.3 ± 0.1	Assuming a rectangular shape ~9.4 × 3.6 × 6.9 Å

[a] The uncertainties are defined by the difference between the average value and the maximum and minimum values measured.

[b] The average diameters have been calculated by averaging the four dimensions (diameters) of the four tetrahedral axes. These tetrahedral dimensions have been calculated using r_{vdw} (H) = 1.30 Å and r_{rdw} (Cl) = 1.80 Å, and bond length extracted from the PC MODEL computer software.

[c] Not accurate since the system is not reversible. However, the few data extracted from the Benesi–Hildebrand plots indicate that K_{11} is very large (>10 000 M^{-1}).

[d] A slow thermal reaction has been observed at high concentrations. At low concentrations (~10^{-3} M in $C_6H_5CH_2Cl$ for ~10^{-5} M in cluster) no reaction is observed.

Table 2. Comparison of Φ_{dis} with E(C—Cl) and $E^{0/-}$.

	Φ_{dis}	E(C—Cl)/kcal mol^{-1}[a]	$E^{0/-}$/V[b]
Cl^-	~1.5×10^{-5}	—	—
	0.86 M (in ethanol)		
Neat C_6H_5Cl	0.00044 ± 0.00010	95 (CRC)	−2.32
Neat CH_2Cl_2	0.00051 ± 0.00023	82.8 (JPC)	−2.23
Neat $CHCl_3$	0.0030 ± 0.0005	79.2 (JPC)	−1,67
Neat CCl_4	0.00080 ± 0.00015	70.3 (JPC)	−0.78, −1.71
1-Cl-ada	0.000048 ± 0.000010	[c]	[d]
	3.43 M (in toluene)		
Neat $C_6H_5CH_2Cl$	Thermal	69 (CRC)	−1.0 (vs.
SCE)[e]			

[a] 1 kcal = 4.18 kJ. From ref. 37.

[b] In 75% dioxane vs. NHE (unless stated otherwise) from ref. 26.

[c] The E(C—Cl) for CH_3CH_2Cl is 81 kcal mol^{-1} (CRC handbook).

[d] $E^{0/-}$ for chlorobicyclo[7,1^{1,5}]heptane is −1.99 V. It is highly suspected that $E^{0/-}$ for 1-Cl-ada is also ~−2 V.

[e] From ref. 27.

by at least one order of magnitude on going from Cl—CH_2Cl (0.25 M^{-1}) to C_6H_5—CH_2Cl (~7.3 M^{-1}) is not unprecedented. The K_{11} increases from acetate to benzoate, nitroethane to nitrobenzene, and acetonitrile to benzonitrile are also all around an order of magnitude (13). Cooperation between the binding of the Cl atom with the Pd_3 center, and the binding of the hydrophobic phenyl group and the cavity dppm-phenyl groups, appears to be responsible for this phenomenon. Finally, the unexpectedly large K_{11} value for 1-Cl-ada can only be explained by a binding involving only the hydrophobic portions of the host–guest pair. In this case the multiple hydrophobic intermolecular contacts could lead to a large K_{11} value. No attempt was made to further investigate this phenomenon.

4. Quantum Yields

The photochemical quantum yields (Φ) were measured by ferrioxalate actinometry following the rate of $Pd_3(dppm)_3CO^{2+}$ consumption by UV–visible spectroscopy (λ_{max} ~ 480 nm). First, $Pd_3(dppm)_3CO^{2+}$ was investigated in neat solvents (Table 2). We noticed that in neat $C_6H_5CH_2Cl$, $Pd_3(dppm)_3CO^{2+}$ reacted slowly (thermally) at room temperature, so no Φ value could be measured. However, at [R—Cl] ~ 10^{-3} M (typical concentration range for K_{11} measurements), no detectable reaction was noticed. This reactivity is tentatively attributed to the relatively high stability of the benzyl radical ($C_6H_5CH_2^{\cdot}$); and it is concluded that the homolytic C—Cl bond cleavage by $Pd_3(dppm)_3CO^{2+}$ is facile in this case. For C_6H_5Cl, CH_2Cl_2, and $CHCl_3$, Φ increases with both the decrease in E(C—Cl) and $E^{0/-}$ values. Surprisingly, Φ decreases for CCl_4 while E(C—Cl) and $E^{0/-}$ continue to decrease in this series. This result further supports the conclusion that the primary process in the mechanism cannot be an

Fig. 3. Graph of $\Phi_{dis}(Pd_3(dppm)_3CO^{2+})$ vs. % $CHCl_3$ (V:V) in toluene (top) and ethanol (bottom).

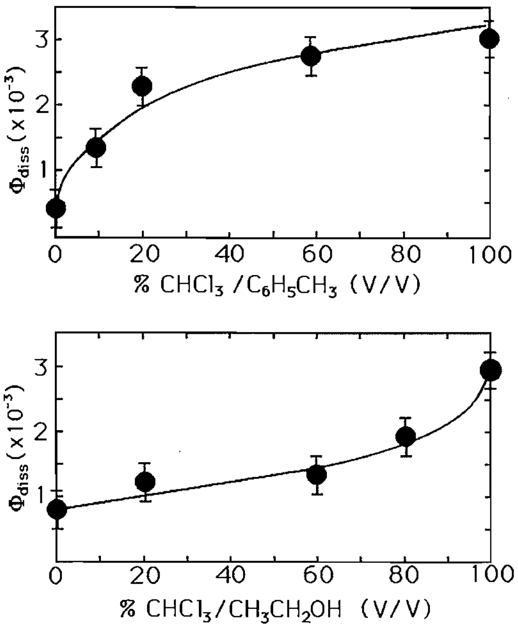

decrease in this series. This result further supports the conclusion that the primary process in the mechanism cannot be an outer-sphere electron transfer. On the other hand, an atom transfer mechanism is not ruled out since "steric considerations" can also affect the rates of reaction. One has to note that the K_{11} data also arise from measurements that also consider the steric effects in the complex stability. By ignoring the experimental uncertainties, Φ varies as $C_6H_5Cl < CH_2Cl_2 < CCl_4 < CHCl_3$ in neat solvents, which parallels the trend in K_{11}. For the chloride substrate, at $[Cl^-] = 0.86$ M (as Bu_4N^+ salt) in ethanol, $\Phi \sim 1.5 \times 10^{-5}$ (extremely weak)! Again no reaction is observed in the dark. One has to note that the Cl^- ion is very strongly bonded to the $Pd_3(dppm)_3CO^{2+}$ cluster, so no direct comparison of the Φ values can be made. The extremely low Φ value indicates that the photodecomposition is slow. This is indeed observed during the bulk photolysis reactions for $Pd_3(dppm)_3(CO)(Cl)^+$ (i.e., the photoproduct of the $Pd_3(dppm)_3(CO)(N_2C_6H_4NEt_2)^{3+}$ photodecomposition in CH_2Cl_2, believed to be one of the intermediates).

For comparison purposes, Φ's for the photochemical reactions between $Pt_3(dppm)_3CO^{2+}$ and $CHCl_3$, and CH_2Cl_2 (neat) were also measured. As expected, the Φ value is greater for M = Pt with $CHCl_3$ ($\Phi = 0.0041 \pm 0.0005$ at λ = 380nm) than that of $Pd_3(dppm)_3CO^{2+}$ (0.0030 ± 0.0005). For CH_2Cl_2, Φ is about the same for both clusters, considering the uncertainties. Both the triplet energy and the excited state driving forces are greater for $Pt_3(dppm)_3CO^{2+}$. These experiments did not provide any evidence of one mechanism or another.

Based upon the hypothesis that an atom transfer mechanism involves a physical approach of the R-Cl molecule towards the M_3 center, Φ should be sensitive to the presence of a competitive molecule (solvent). Figure 3 shows the relationship of Φ for the $Pd_3(dppm)_3CO^{2+}$–$CHCl_3$ photoreactions as a function of the % (V/V) for two different solvents (toluene and ethanol). The toluene graph shows an upward curvature, while the ethanol graph shows a downward curvature, with the increase in %(V/V), in $CHCl_3$, confirming the expected difference. Except for CH_2Cl_2, the other substrates were not investigated as a function of %(V/V) substrate and solvent. For CH_2Cl_2, Φ increases (slightly) with % (V/V) CH_2Cl_2, but the large uncertainties prevent us from determining the curvature trend. Based upon the K_{11} measurements reported elsewhere (13), ethanol appears to be a better binder than toluene with $Pd_3(dppm)_3CO^{2+}$. Figure 3 indicates that ethanol inhibits the increase in Φ values with the increase in $[CHCl_3]$. On the other hand, the sharp increase in Φ's in the toluene graph at low $[CHCl_3]$ indicates that toluene does not efficiently inhibit the photoreactions. These results are also consistent with this substrate–cavity model where toluene does not compete as efficiently as ethanol for the cavity.

Scheme 2.

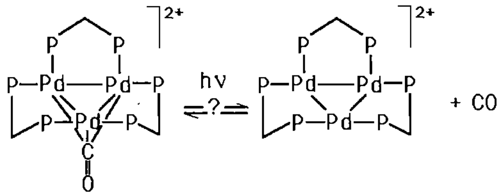

The most surprising result is the non-zero value at 0% quantity of $CHCl_3$ (~0.0005), indicating that $Pd_3(dppm)_3CO^{2+}$ is photo-consumed even in the absence of chlorocarbons. We note that these values are even greater than that of the Cl^- substrate stated above. This observation clearly indicates the presence of a second photochemical pathway since with short periods of time in the dark, this instability does not occur. This pathway is clearly inefficient with such low quantum yields, but cannot be neglected for the CH_2Cl_2, CCl_4, 1-Cl-ada, and C_6H_5Cl substrates. The design of experiments in order to elucidate this second pathway is not obvious. Two proposed mechanisms can be anticipated: (*i*) photolabilisation of the CO group (Scheme 2) as observed in many organometallic polynuclear complexes (1) followed by a breakdown of the cluster, and (*ii*) photoinduced fragmentation of the cluster according to eq. [2]:

$$[2] \quad Pd_3(dppm)_3CO^{2+} \underset{\text{dark}}{\overset{h\nu}{\rightleftarrows}} \text{"}Pd(dppm)\text{"} + \text{"}Pd_2(dppm)_2(CO)(S)_2{}^{2+}\text{"} \longrightarrow \text{products}$$

where S is a two-electron donor (counter anion or solvent molecule). This second reaction is essentially the last step prior to the synthesis of the $Pd_3(dppm)_3CO^{2+}$ cluster as demonstrated by Puddephatt and co-workers (7, 8). The following experiments are performed: (*i*) measurements of Φ in the presence of CO(g), and (*ii*) measurements of Φ for the PF_6^- and $CF_3CO_2^-$ salts. The first set of experiments (Φ vs. CO(g)) demonstrates that Φ is independent (within the experimental uncertainties) in the presence of 1 atm of CO(g) (1 atm = 101.3 kPa). The synthesis of $Pd_3(dppm)_3CO^{2+}$ does not require high pressures of CO (7). This experiment was attempted in order to slow down the CO loss, if any. The most revealing experiments are the measurements of Φ for $Pd_3(dppm)_3CO^{2+}$ as a PF_6^- and as a $CF_3CO_2^-$ salt. Using different solvents (ethanol and acetonitrile) and atmospheres (Ar, CO_2, O_2, CO, and H_2), we find that

Scheme 3.

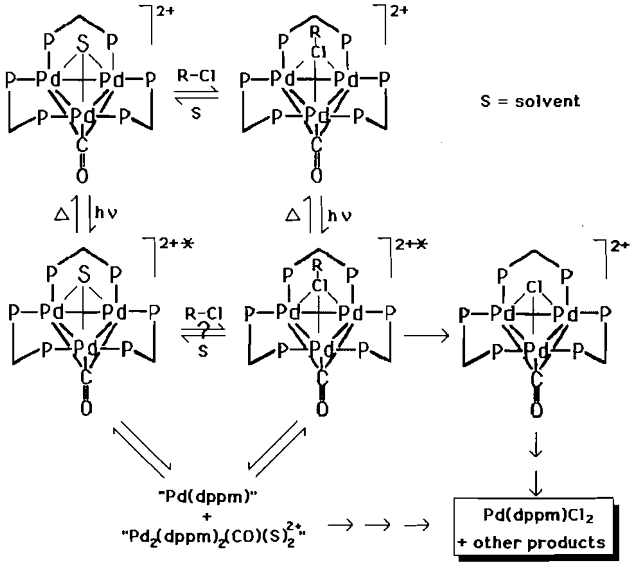

is a better binder than PF_6^- (13) which should indicate that the cavity is competitively blocked by the carboxylate molecule, if one assumes the host–guest mechanism. However, this result is consistent with eq. [2] shifting the reaction to the right when S is a better two-electron donor. Interestingly we find Φ (ethanol) > Φ (toluene) (at [substrate] = 0, see Fig. 3), where ethanol is a two-electron donor. The next question is whether or not the formation of $Pd_3(dppm)_3^{2+}$ (first scenario: Scheme 2) can lead to an *efficient* subsequent fragmentation of the cluster. Theory predicts that it cannot (see section below), corroborating the experimental results (Φ vs. CO(g)). Then, will the intermediates generated in eq. [2] subsequently react with R—Cl to produce the final observed products? Previous studies strongly indicate that it is indeed possible. The highly reactive "Pd(dppm)" species is expected to be thermally active towards R—Cl based upon the known chemistry for "$Pd(R_2PCH_2CH_2PR_2)$" where R = C_6H_{11} (28). For the CO bridged d^9-d^9 proposed intermediates (eq. [2]), a recent work on an isoelectronic CNR bridged "$Pd_2(dppm)_2$" d^9-d^9 compound demonstrated that this complex was efficiently photoconverted to $Pd(dppm)Cl_2$ in the presence of CH_2Cl_2 (29). Thus, experimental and literature results favor scenario (*ii*) for the second pathway of R—Cl activation. The overall proposed pathways are summarized in Scheme 3. The C—Cl homolytic bond cleavage involves the formation of the $Pd_3(dppm)_3(CO)(Cl)^{2+}$ intermediate, which represents one of the mechanistic steps of the photoinduced photodegradation of the cluster.

Considering the K_{11} measured for 1-Cl-ada, one would expect Φ to be large. However, the binding does not necessarily involve the C-Cl bond oriented inside the cavity. Indeed, Φ(1-Cl-ada) = 0.000048 ± 0.000010 for [1-Cl-ada] = 3.43 M in toluene. This value is by far the smallest one (excluding the Cl^- case). Further, the CPK models demonstrate that the bulkiness of 1-Cl-ada precludes strong $R—Cl\cdot\cdot Pd_3^{2+}$ interactions, confirming that homolytic bond cleavage by $Pd_3(dppm)_3CO^{2+*}$ ($^3A_2$) is not anticipated to be efficient.

5. Emission lifetimes

This section addresses the first proposed pathway (host–guest chemistry). Perturbation studies of the photophysical properties of the $M_3(dppm)_3CO^{2+}$ complexes indicate that the presence of a substrate in the cavity always induces a decrease in excited state lifetimes (25). This general behavior has also been observed for metal complexes of calix[4]arene derivatives for which a metal atom is located at the lower rim acting either as a luminescent probe (Ir(I); ref. 30) or a strong Lewis acid (W = O (31)), and the recently investigated $Cu_3(dppm)_3OH^{2+}$ cluster (32). This phenomenon is attributable to the "loose bolt effect" (for small perturbations) or to the formation of an "exciplex" (for larger change in lifetimes) (33). For $Pt_3(dppm)_3CO^{2+}$ both 298 K flash photolysis and 77 K emission lifetime measurements established that toluene as a pure solvent provided the shortest lifetimes among the solvent molecules investigated (25). The hypothesis is that toluene binds more strongly to $Pt_3(dppm)_3CO^{2+}$ than do most common solvents. This difference with $Pd_3(dppm)_3CO^{2+}$ is not understood at this time.

To further understand the difference between the photochemical quantum yield behavior in toluene and ethanol, the emission decay traces for $Pt_3(dppm)_3CO^{2+}$ at 77 K in the presence of CH_2Cl_2 and $CHCl_3$ were investigated. $Pt_3(dppm)_3CO^{2+}$ was selected because of its greater emission quantum yield at 77 K (34). At such a temperature, cluster degradation is not anticipated to be an inefficient mechanism for the excited state deactivation; solely the $Pt_3^{2+}\cdots Cl—R$ interactions are governing the changes in τ_e with [Cl—R]. In pure solvent, the emission decays are rigorously monoexponential (τ_e = 10.2 ± 0.5 μs, toluene; τ_e = 18.0 ± 0.1 μs, ethanol). In the presence of $CHCl_3$ or CH_2Cl_2, the carefully measured decays become biexponential (Fig. 4). The biexponential behavior is demonstrated from deconvolution decay analysis. The emission spectra exhibit no band shift but show a gradual decrease in intensity with chlorocarbon concentration. The long component exhibits a τ_e value of 10.2 or 18.0 μs characteristic of the solvent, and does not change (within ±0.5 μs) with an increase in chlorocarbon concentration up to 40% (V/V). Such a result further rules out the possibility of an outer-sphere electron transfer in the excited state in these cases ($CHCl_3$, CH_2Cl_2), since generally the emission decay traces exhibit monoexponential behaviors with lifetimes decreasing with the substrate concentration. The short component exhibits a lifetime of 450 ± 150 ns for both CH_2Cl_2 and $CHCl_3$. The relative intensity ratio for short component/long component after deconvolution increases proportionally with the chlorocarbon/solvent ratio (V/V). This experiment demonstrates that the short and long components are associated with the luminescence of $Pt_3(dppm)_3CO^{2+}$ interacting (or hosting) a chlorocarbon and a solvent molecule, respectively. The very short lifetimes in the $Pt_3(dppm)_3CO^{2+}\cdots$ chlorocarbon cases strongly indicate the formation of exciplexes. The exciplex emissions appear to be weak since the emission intensity of the mixture steadily decreases with the increase in chlorocarbon concentration. Also these emissions are anticipated to be located very close to the $Pt_3(dppm)_3CO^{2+}\cdots$ solvent emissions, since no change in λ_{max} emission was observed in all the experiments. The most important finding is that the short component/long component intensity ratio always differs greatly between the two solvents (ethanol, toluene) at a given chloro-

Fig. 4. Typical emission decay traces for the $Pt_3(dppm)_3CO^{2+}$ clusters at 77 K. Top: in toluene containing 30% CH_2Cl_2 (V:V) Bottom: in ethanol containing 3% CH_2Cl_2 (V:V). The peaks marked with an X are instrumental artifacts. The double arrow markings indicate the short-lived components (~18% of the total intensity).

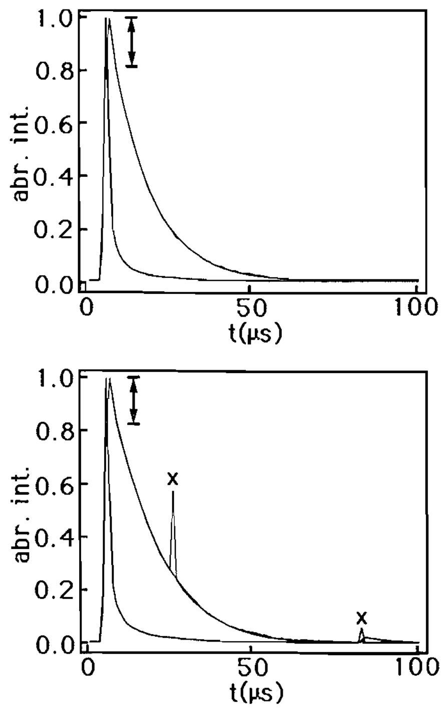

Fig. 5. Optimized ground state geometry of the model compound $Pd_3(PH_3)_6(CO)(Cl)^+$. The geometry for $Pd_3(PH_3)_6(CO)(Cl)^{2+}$ is the same except that some distances and angles have changed (see details in Table 4).

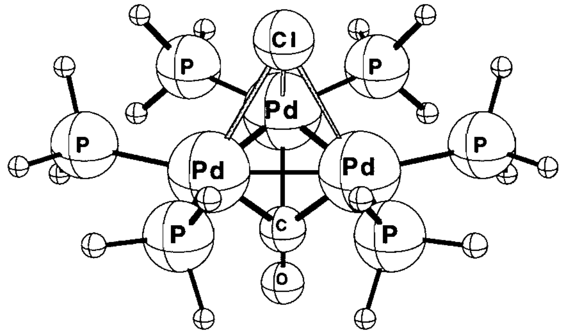

Fig. 6. Optimized geometry of the model association complex $Pd_3(PH_3)_6(CO)^{2+}\cdots ClCH_3$ in the ground state.

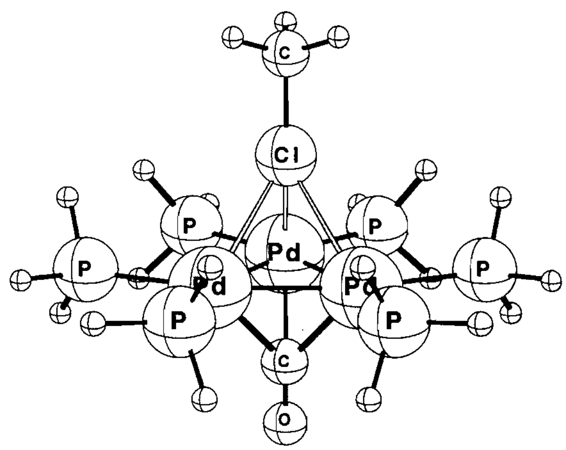

carbon/solvent ratio. As a typical example, Fig. 4 compares two 77 K emission decays of $Pt_3(dppm)_3CO^{2+}$: the first in toluene containing 30% CH_2Cl_2, and the second in ethanol containing 3% CH_2Cl_2. Both decays exhibit the same short component/long component ratio (~18%). This result indicates that the halocarbon molecule competes relatively more efficiently to occupy the $Pt_3(dppm)_3CO^{2+}$ cavity in ethanol. Essentially, this confirms that ethanol is a weaker binder for $Pt_3(dppm)_3CO^{2+}$ than toluene and further supports the above hypothesis.

6. Geometry optimizations

Density functional theory was used to optimize geometries in the ground state of some proposed intermediates in order to explain and corroborate some experimental results. For $Pd_3(dppm)_3CO^{2+}$ in its ground ($^1A_1$) and lowest energy triplet excited states ($^3A_2$, (T_1), $^3E_2$ (T_2)), the geometry compounds have already been computed (35). The computations compared very favorably with the experimental data, particularly for the Pd—Pd bond lengths. For comparison purposes, these data are reported in Table 3. The geometry of the model $Pd_3(PH_3)_6(CO)(Cl)^+$ cluster has also been optimized (Table 3 and Fig. 5) in order to address the weak interactions between the Pd_3^{2+} center and the substrate. The comparison of the Pd—Pd bond lengths is also excellent, but some differences are noted for the covalent Pd—P and Pd—C bonds. These differences can be up to 0.055 Å. For the more ionic Pd···Cl interactions, the computed Pd···Cl distance is significantly shorter than that of the crystal structures. The differences are up to 0.23–0.26 Å from the average X-ray values. Steric effects with the H-dppm atoms and the nature of the theoretical methods employed are likely to be at the origin of these differences. Investigations should concentrate mainly on the metal–metal bonds.

The first optimization considered is the ground state interactions between $Pd_3(PH_3)_6CO^{2+}$ and chloromethane (Fig. 6). The number of atoms is kept low in order to reduce the computer time, and the optimization was performed under the restricted C_{3v} symmetry. The results of the computations are compared in Table 4. The first and most important prediction is that the Pd···Cl interactions are expected to be very weak as the computed Pd···Cl distances are in the order of 2.83 Å. This distance compares to average distances of the X-ray results reported for $Pd_3(dppm)_3(CO)(Cl)^+$ (Table 3), but is in fact larger than that of the $Pd_3(PH_3)_6(CO)(Cl)^+$ computed distance (2.628 Å). This result may be due to the lack of electrostatic interaction between Pd_3^{2+} and neutral $ClCH_3$. The calculated Pd—Pd bond length (2.63 Å) compares favorably to that of most "$Pd_3(dppm)_3CO^{2+}$" complexes reported so far (see ref. 36 for examples). The r(Pd—P), r(C═O), and r(Pd—C) calculated values also compare with the $Pd_3(PH_3)_6(CO)(Cl)^+$ and

$Pd_3(PH_3)_6(CO)^{2+}$ data. We conclude that the interactions between the Cl atom of R—Cl and the Pd_3^{2+} center is very weak, causing little perturbation to the host skeleton. The following set of calculations addresses the possibility of the photoinduced labilization of CO (Scheme 2). The optimized geometry of $Pd_3(PH_3)_6^{2+}$ was calculated and the results at convergence (Table 4) indicate that the Pd—Pd and Pd—P distances undergo practically no, or very little, perturbation (within 0.03 Å). If the Pd—Pd bond length had significantly increased, one may have suspected that fragmentation would occur. This is not the case.

To shed light on the steps following the homolytic C—Cl bond cleavage, the geometries of the model compounds $Pd_3(PH_3)_6CO^{3+}$ and $Pd_3(PH_3)_6(CO)(Cl)^{2+}$ were also investigated. The question is, what may happen after the $Cl^{\cdot}$ radical starts interacting with the Pd_3^{2+} center? One hypothesis is an intramolecular electron transfer from the Pd_3^{2+} center to the strongly oxidant $Cl^{\cdot}$ radical. To test this hypothesis, the structure of the $Pd_3(PH_3)_6CO^{3+}$ compound is optimized (Table 4). While the *r*(Pd—P), *r*(C˙O), and *r*(Pd—C) data resemble the rest of the data reported in Table 4, the calculated Pd—Pd distance has significantly increased to ~2.73 Å. This distance is very close to the limit of a formal Pd—Pd single bond (see data reported in ref. 3). It is also close to the distance found experimentally in the $Pd_3(dppm)_3CO^{2+}$ cluster in its lowest energy triplet excited state ($^3A_2$; ~2.78 Å) (35). If a formal electron is indeed transferred from the Pd_3^{2+} to the $Cl^{\cdot}$ center to form the Pd_3^{3+} and Cl^- species, then the calculated Pd—Pd bond length in $Pd_3(PH_3)_6(CO)(Cl)^{2+}$ should be close to 2.73 Å also. This is not quite the case as the computed distance converges to 2.68 Å, indicating that the structure is an intermediate between the two forms ($Pd_3^{2+}\cdots Cl^{\cdot}$ and $Pd_3^{3+}\cdots Cl^-$). The *r*(Pd—P), *r*(Pd—C), and *r*(C═O) data are also "normal" (Table 4), but the Pd···Cl distance has significantly decreased, down to ~2.54 Å. This increase in interactions may appear to be due to an increase in electrostatic interactions (i.e., $Pd_3^{3+}\cdots Cl^-$ form). Nonetheless, with a distance of ~2.68 Å typical for a Pd—Pd dppm bridged single bond, the homolytic scission of the Pd—Pd bond after the Cl abstraction does not seem obvious at this point. However, the electrochemical cyclic voltammograms recorded for both $M_3(dppm)_3CO^{2+}$ clusters (M = Pd,Pt) exhibit irreversible oxidation waves, suggesting that further events are obviously taking place after the transfer of the first electron ($Pd_3^{2+} \rightarrow Pd_3^{3+} + 1e^-$). The intramolecular electron transfer between the Pd_3^{2+} and $Cl^{\cdot}$ centers forming Pd_3^{3+} and Cl^-, which subsequently degrade into products, still appears as a possible mechanism of photoinduced fragmentation.

Final remarks

The photoinduced degradation of $M_3(dppm)_3CO^{2+}$ in the presence of chlorocarbons and chloride ion proceeds via very complicated pathways. This work has addressed only a fraction of them, notably for the primary steps. There is no evidence of an electron transfer mechanism involving the excited clusters in their $^3A_2$ states and the R—Cl and Cl^- substrates. On the other hand, the series of measurements performed were all consistent with an atom abstraction mechanism. The well-established host–guest behavior of the cluster was used to confirm this mechanism in the $^3A_2$ states. To our knowledge such a strategy does not seem to have been employed before.

Table 3. Comparison of the calculated and experimental structures for Pd_3 clusters (bond lengths in Å).

	$Pd_3(PH_3)_6CO^{2+}$ ground state calculated	$Pd_3(dppm)CO^{2+}$ X-ray[a]	$Pd_3(PH_3)_6CO^{2+}$, $^3A_2$, calculated[b]	$Pd_3(dppm)_3CO^{2+}$, $^3A_2$ excited state distortion[b]	$Pd_3(PH_3)_6(CO)(Cl)^+$ calculated	$Pd_3(dppm)_3(CO)(Cl)^+$ Puddephatt (X-ray)[c]	$Pd_3(dppm)_3(CO)(Cl)^+$ This work (X-ray)
r(Pd—Pd)	2.592	2.604(30)	2.778	~2.78	2.594	2.591(11)	2.595(17)
r(Pd—C)	2.317	2.318(30)	2.376	—	2.287	2.310(11)	2.311(30)
r(Pd—C)	2.080	2.105(17)	2.057	—	2.189	?	2.244
r(C═O)	1.170	1.165(5)	1.169	—	1.156	?	[d]
r(Pd—Cl)					2.628	2.741 2.796 3.161 2.899(average)	2.668 2.903 3.011 2.861(average)

[a] These data are taken from ref. 13.
[b] These data are taken form ref. 35.
[c] From ref. 24, and CSD (Cambridge Structural Database).
[d] This value is fixed in the refinement.

Table 4. Comparison of the calculated structures for Pd_3 clusters (bond lengths in Å).[a]

	$Pd_3(PH_3)_6^{2+}$	$Pd_3(PH_3)_6CO^{3+}$	$Pd_3(PH_3)_6(CO)(Cl)^{2+}$	$Pd_3(PH_3)_6(CO)(Cl)^{+}$	$Pd_3(PH_3)_6(CO)(ClCH_3)^{2+}$	$Pd_3(PH_3)_6(CO)^{2+}$
r(Pd—Pd)	2.606	2.733	2.680	2.594	2.634	2.592
r(Pd—P)	2.191	2.335	2.331	2.287	2.317	2.317
r(C═O)	—	1.157	1.161	1.156	1.158	1.170
r(Pd—d)	—	2.097	2.115	2.189	2.117	2.080
r(Pd—Cl)	—	—	2.541	2.628	2.830	—

[a] Data for $Pd_3(PH_3)_6(CO)(Cl)^+$ are also compared in Table 3, and data for $Pd_3(PH_3)_6(CO)^{2+}$ are from ref. 35. All calculations were performed under a C_{3v} restricted geometry.

One very important observation is clearly the very low photochemical quantum yields, demonstrating the rather inefficient capacity of the clusters to photoactivate the C—Cl bond. For stronger C—X bonds (such as C—H), this observation allows us to predict that the cleavage of this C—X bond will simply not occur, but rather the second pathway (primary photoinduced fragmentation of the cluster) may become dominant in order to promote reactivity in these cases. Thus cluster degradation and decomposition should be observed. This is consistent with the nature of the organic photoproducts observed with the chloride substrate, which are all phosphine derivatives (issued from the coordinated dppm). This decomposition mechanism is complex since high molecular weight fragments are observed (higher than dppm in some cases), indicating that the processes involved formation of free radicals. The very low photochemical quantum yields (Φ) have been commented on in one of our studies on O_2 activation (6). There are many possible explanations for the low Φ values: (*i*) the excited state lifetimes are found to be extremely short ($\tau_1 < 40$ ps, M = Pd; $\tau_1 < 40$ ps, $70 < \tau_2 < 400$ ns, intensity ratio for $\tau_1/\tau_2 = 95/5$, M = Pt; (ref. 25)); (*ii*) access to the lumophore is sterically hindered by another interacting substrate in the ground and excited states; and (*iii*) the biradical-type excited state is delocalized over three metal centers, not localized as in the case of the $M_2(CO)_{10}$ dimers ($2 \times M(CO)_5$; M = Mn, Re; ((ref. 1*a*)). Further studies in this area are in progress.

Acknowledgements

This research was funded by the Natural Sciences and Engineering Research Council of Canada (NSERC) and FCAR (Fonds concertés pour l'avancement de la recherche). J.G. is grateful to FCAR and R.P. to the Université de Sherbrooke for the award of graduate scholarships. P.D.H. also thanks Professor Yves Mugnier (Université de Bourgogne, Dijon) for kindly measuring the cyclic voltammograms of the two clusters (as PF_6 salts).

References

1. (*a*) G.L. Geoffroy and M.S. Wrighton. Organometallic photochemistry. Academic Press, New York. 1979; (*b*) T.J. Meyer and J.V. Caspar. Chem. Rev. **85**, 187 (1985); (*c*) P. D. Harvey. J. Cluster. Sci. **4**, 377 (1993).
2. D. Perreault, M. Drouin, A. Michel, and P.D. Harvey. Inorg. Chem. **31**, 2740 (1992).
3. P.D. Harvey and Z. Murtaza. Inorg. Chem. **32**, 4721 (1993).
4. F.R. Lemke, R.M. Granger, D.A. Morgenstern, and C.P. Kubiak. J. Am. Chem. Soc. **112**, 4052 (1990).
5. (*a*) P.A. Metcalf and C.P. Kubiak. J. Am. Chem. Soc. **108**, 4682 (1986); (*b*) M.K. Reinking, M.L. Kullberg, A.R. Culter, and C.P. Kubiak. J. Am. Chem. Soc. **107**, 3517 (1985).
6. P.D. Harvey, M. Crozet, and K.T. Aye. Can. J. Chem. **73**, 123 (1995).
7. L. Manojlovic-Muir, K.W. Muir, B.R. Lloyd, and R.J. Puddephatt. J. Chem. Soc. Chem. Commun. 1336 (1983).
8. G. Ferguson, B.R. Lloyd and R.J. Puddephatt. Organometallics, **5**, 344 (1986).
9. H.J. Kuhn, S.E. Braslavsky, and R. Schmidt. Pure Appl. Chem. **61**, 187 (1989).
10. S.L. Murov, I. Carmichael, and G.L. Hug. Handbook of photochemistry. 2nd ed. Marcel Dekker, Inc., New York. 1993. pp. 299–301.
11. E.E. Wegner and A.W. Adamson. J. Am. Chem. Soc. **88**, 394 (1966).
12. K.A. Connors. Binding constants: the measurement of molecular complex stability. J. Wiley & Sons, New York. 1987.
13. R. Provencher, K.T. Aye, M. Drouin, J. Gagnon, N. Boudreault, and P.D. Harvey. Inorg. Chem. **33**, 3689 (1994).
14. E.J. Baerends, D.E. Ellis, and P. Ros. Chem. Phys. **2**, 41 (1973).
15. E.J. Baerends. Ph.D. Thesis, Vrije Universiteit, Amsterdam (1975).
16. W. Raveneck. Algorithms and applications on vector and parallel Computers. *Edited by* H.J.J. Rigie, Th. J. Dekkor, and H.A. van de Vorst. Elsevier, Amsterdam. 1987.
17. P.M. Boerrigter, G. te Velde, and E.J. Baerends. Int. J. Quantum Chem. **33**, 87 (1988).
18. L. Verluis and T. Ziegler. J. Chem. Phys. **88**, 322 (1988).
19. (*a*) G.J. Snijders, E.J. Baerends, and P. Vernooÿs. At. Nucl. Data Tables, **26**, 483 (1982); (*b*) P. Vernooÿs, G.J. Snijders, and E.J. Baerends. J. Int. Slater Type Basis Functions for the Whole Periodic System; Internal Report. Free University of Amsterdam, Amsterdam. 1981.
20. (*a*) L. Noodleman and J.G. Nownan. J. Chem. Phys. **70**, 4903 (1979); (*b*) L. Noodleman. J. Chem. Phys. **74**, 5737 (1981); (*c*) L. Noodleman and E.J. Baerends. J. Am. Chem. Soc. **106**, 2316 (1984).
21. J. Krijn and E.J. Baerends. *In* Fit function in the HFS method, Internal Report (in Dutch). Free University of Amsterdam, Amsterdam. 1984.
22. S.D. Vosko, L. Wilk, and M. Nusair. Can. J. Phys. **58**, 1200 (1990).
23. (*a*) Y. LePage, P.D. White, and E.J. Gabe. NRCCAD. An enhanced CAD-4 control program. Proc. Am. Crystallogr., Hamiton Meeting, 1986, Abstract PA 23; (*b*) E.J. Gabe, Y. LePage, J.-P. Charland, F.L. Lee, and P.S. White. J. Appl. Crystallogr. **22**, 384 (1989); (*c*) C.K. Johnson. ORTEP — A Fortran thermal ellipsoid

ploprogram. Technical Report ORNL-5138, Oakridge, Tenn. 1976.

24. L. Manojlovic-Muir, K.W. Muir, B.R. Lloyd, and R.J. Puddephatt. J. Chem. Soc. Chem. Commun. 536 (1985).
25. P.D. Harvey, S.M. Hubig, and T. Ziegler. Inorg. Chem. **33**, 3700 (1994).
26. M.R. Rifi and F.H. Covitz. Introduction to organic chemistry. Marcel Dekker, New York 1974. pp. 200–204.
27. P. Zuman. Handbook series in organic electrochemistry. Vol. 1. CRC Press, Inc., Cleveland, Ohio. 1977. p. AG22.
28. Y. Pan, J.T. Mague, and M.J. Fink. J. Am. Chem. Soc. **115**, 3842 (1993).
29. M.A. Khan and A.J. McAlees. Inorg. Chim. Acta, **104**, 109 (1985).
30. J. Gagnon, C. Loeber, D. Matt, and P.D. Harvey. Inorg. Chim. Acta. **242**, 137 (1996).
31. P.D. Harvey, J. Gagnon, R. Provencher, B. Xu, and T. Swager. Can. J. Chem. **74**, 000 (1996).
32. R. Provencher and P.D. Harvey. Inorg. Chem. **35**, 2235 (1996).
33. N.J. Turro. Modern molecular photochemistry. The Benjamin/Cummings Publishing Co. Inc., Menlo Park, Calif. 1978, pp. 138 and 172.
34. R. Provencher and P.D. Harvey. Inorg. Chem. **32**, 61 (1993).
35. R. Provencher and P.D. Harvey. Inorg. Chem. **35**, 2113 (1996).
36. R.J. Puddephatt, L. Manojlovic-Muir, and K.W. Muir. Polyhedron, **9**, 2767 (1990).
37. (*a*) R.C. Weast, D.R. Lide, M.J. Astle, and W.H. Beyer (*Editor*). CRC handbook of chemistry and physics. 75th ed. CRC Press, Boca Roton, Fla. 1995. p.F. 234; (*b*) M. Weissman and S.W. Benson. J. Phys. Chem. **87**, 243 (1983).